Int J Biometeorol (2015) 59:237–248
DOI 10.1007/s00484-014-0839-z

ORIGINAL PAPER

Determining the relative importance of climatic drivers on spring phenology in grassland ecosystems of semi-arid areas

Likai Zhu · Jijun Meng

Received: 27 December 2013 / Accepted: 19 April 2014 / Published online: 7 December 2014

Abstract Understanding climate controls on spring phenology in grassland ecosystems is critically important in predicting the impacts of future climate change on grassland productivity and carbon storage. The third-generation Global Inventory Monitoring and Modeling System (GIMMS3g) normalized difference vegetation index (NDVI) data were applied to derive the start of the growing season (SOS) from 1982–2010 in grassland ecosystems of Ordos, a typical semi-arid area in China. Then, the conditional Granger causality method was utilized to quantify the directed functional connectivity between key climatic drivers and the SOS. The results show that the asymmetric Gaussian (AG) function is better in reducing noise of NDVI time series than the double logistic (DL) function within our study area. The southeastern Ordos has earlier occurrence and lower variability of the SOS, whereas the northwestern Ordos has later occurrence and higher variability of the SOS. The research also reveals that spring precipitation has stronger causal connectivity with the SOS than other climatic factors over different grassland ecosystem types. There is no statistically significant trend across the study area, while the similar pattern is observed for spring precipitation. Our study highlights the link of spring phenology with different grassland types, and the use of coupling remote sensing and econometric tools. With the dramatic increase in global change research, Granger causality method augurs well for further development and application of time-series modeling of complex social–ecological systems at the intersection of remote sensing and landscape changes.

Keywords Ordos · Semi-arid area · Grassland · Land surface phenology · The start of the growing season (SOS) · Climate change

Introduction

Phenology is the study of the timing of recurring biological cycles and their connection to climate (White et al. 1997, 2009). Vegetation phenology can influence the exchange of energy, water vapor, and momentum between the land surface and the atmosphere and, therefore, is critical for the global carbon and water cycle (Luo et al. 2013; Cong et al. 2013). Vegetation phenology can serve as one of the most important biological indicators of the effects of climate change on biological systems (Dai et al. 2013b). An earlier occurrence of spring phenology has been observed in the northern latitudes, which correlates with rising temperatures, either using satellite observations (Myneni et al. 1997; White et al. 2009; Cong et al. 2013) or in situ stations (Menzel and Fabian 1999; Parmesan and Yohe 2003; Menzel et al. 2006; Ma and Zhou 2012; Dai et al. 2013a, b). Thoroughly understanding vegetation phenology and its linkage to climate is essential to incorporate phenology in biogeochemical models and further accurately predict future ecosystem changes (Ge et al. 2013; Wu and Liu 2013).

With the applications of remote sensing in monitoring and characterizing vegetation phenology, we usually used the term land surface phenology (LSP) to refer to the seasonal pattern of variation in vegetated land surfaces observed particularly from remote sensing. LSP is distinguished from plant

Electronic supplementary material The online version of this article (doi:10.1007/s00484-014-0839-z) contains supplementary material, which is available to authorized users.

L. Zhu
Department of Geography, University of Florida, 3141 Turlington Hall, Gainesville, FL 32611, USA
e-mail: likaizhu@ufl.edu

J. Meng (✉)
College of Urban and Environmental Sciences, Peking University, Beijing 100871, China
e-mail: jijunm@pku.edu.cn

phenology which refers to specific life cycle events such as budburst, flowering, or leaf senescence using in situ observations of individual plants and species (de Beurs and Henebry 2010). LSP is based upon "wall-to-wall" observations of phenology at larger geographic scales instead of plant-specific observations. The relationship between satellite measures of LSP and specific plant phenophases is still ambiguous (de Beurs and Henebry 2010). For this reason, the terms about phenological metrics in LSP as well as the methods to derive these metrics are diverse. For example, the terms such as green-up date, leaf-unfolding, green wave, and the start of the growing season (SOS) appear to be interchangeable in the literature (White et al. 2009). Here, we adopted the term SOS which most authors use to represent the phenophase in spring. Since the key LSP metrics are primarily based on time-series analysis of vegetation indices (VI) from optical sensors, the SOS is usually defined as the day of the year (DOY) that the VI reaches the greatest temporal increase. To be specific, two steps are usually applied to identify the SOS using satellite-derived variables such as normalized difference vegetation index (NDVI), enhanced vegetation index (EVI), and normalized difference water index (NDWI) (Zhang et al. 2005; White et al. 2009; Cong et al. 2012, 2013). The first step is to depress the noise and fit the shape of the VI curve using methods such as curving fitting, harmonic analysis, and piecewise functions (Jönsson and Eklundh 2002, 2004; de Beurs and Henebry 2010; Atkinson et al. 2012; Cong et al. 2012). The second step is to calculate the DOY that the VI increases most quickly. The SOS can be determined from the DOY that the VI crosses a specific threshold in an upward direction (White et al. 2009), the DOY when the positive derivative of the VI curve reaches the highest point (Cong et al. 2012, 2013), or the DOY that the first local maxima of the curvature of the VI curve appears (Zhang et al. 2005). Each method has its advantages and limitations. Such differences among methods might lead to the lack of consensus in derived information, uncertainty, and bias between users (Atkinson et al. 2012). To account for the potential uncertainty, White et al. (2009) and Cong et al. (2012, 2013) conduct a multi-method research to quantify changes in vegetation phenology, and conclude that it would be difficult to find a single method suitable for all the vegetation types of diverse landscapes. Besides multi-method study, it is also important to make comparative analysis of these methods using specific measures, particularly when validation data are unavailable.

To our knowledge, greater efforts have been made to investigate the variations in phenology of temperate deciduous forests (tree species) and Qinghai-Tibetan Plateau (grasslands, meadows, and shrubs) (Chen et al. 2005; Piao et al. 2006, 2011; Cong et al. 2012, 2013; Dai et al. 2013a, b; Luo et al. 2013; Zhang et al. 2013), but few exclusively focus on LSP of grasslands in arid and semi-arid areas. These areas have an annual precipitation range of 200–400 mm with high intra- and inter-annual variations. For example, Zhu and Meng (2010) have reported that mean annual precipitation in the 1980s and 1990s is lower than that in the 1960s and 1970s in the middle part of Inner Mongolia, China. Ecosystems in arid- and semi-areas are particularly sensitive to changes of precipitation regimes. Many studies have found a significant positive correlation between NPP and precipitation in water-limited ecosystems (Zhu and Southworth 2013). Peng et al. (2013) have also reported that precipitation amount, seasonality, and frequency can regulate the carbon cycling of semi-arid grassland ecosystems. It is also worth investigating spring phenology of grassland ecosystems and its linkage to climate, which will be useful in understanding the response of terrestrial ecosystems to climate change. Using Ordos, a semi-arid landscape as the study area, our study investigated spatial and temporal variations in the SOS and quantified their relationships with climatic drivers. To be specific, we address the following research questions: (1) Which technique is more appropriate to estimate the SOS in the study area? (2) How has the SOS changed spatially and temporally from 1982–2010? (3) What is the relative importance of climatic drivers in determining the SOS? Our study is critical to predict the impacts of future climate change on LSP, and on the productivity and carbon cycling of grassland ecosystems.

Materials and methods

Study area

The Ordos, which spans from 106°42′E to 111°27′E and 37°35′N to 40°51′N, is a region with relatively independent geographic features in semi-arid areas of China (Fig. 1). The elevation ranges from 1,000–1,500 m and decreases from west to east. This region consists of diverse landforms with a plateau in the west, densely distributed gullies eroded by rivers in the east, a flooding plain in the north, and deserts in the center and south. The entire area exhibits a typical temperate continental climate, with a mean annual precipitation range of 170–350 mm and a mean annual temperature range of 5.3–8.7° C. The total amount of precipitation decreases noticeably from east to west, and rainfall is mainly distributed in July and August. The dominant vegetation is grassland, accounting for about 83.1 % of the study area. Grassland can be subdivided into typical grassland, desert steppe, and meadow (Fig. 1). Typical grassland is a type of zonal vegetation of temperate continental climate in arid- and semi-areas. Desert steppe is a grassland type transitioning from typical grasslands to deserts. They are usually distributed inland with mean annual precipitation less than 200 mm. Meadow is a kind of azonal vegetation, which is composed of perennial grasses. It grows in the semi-humid areas with abundant water. Deserts accounts for 9.6 % of the entire study area. The major parts of

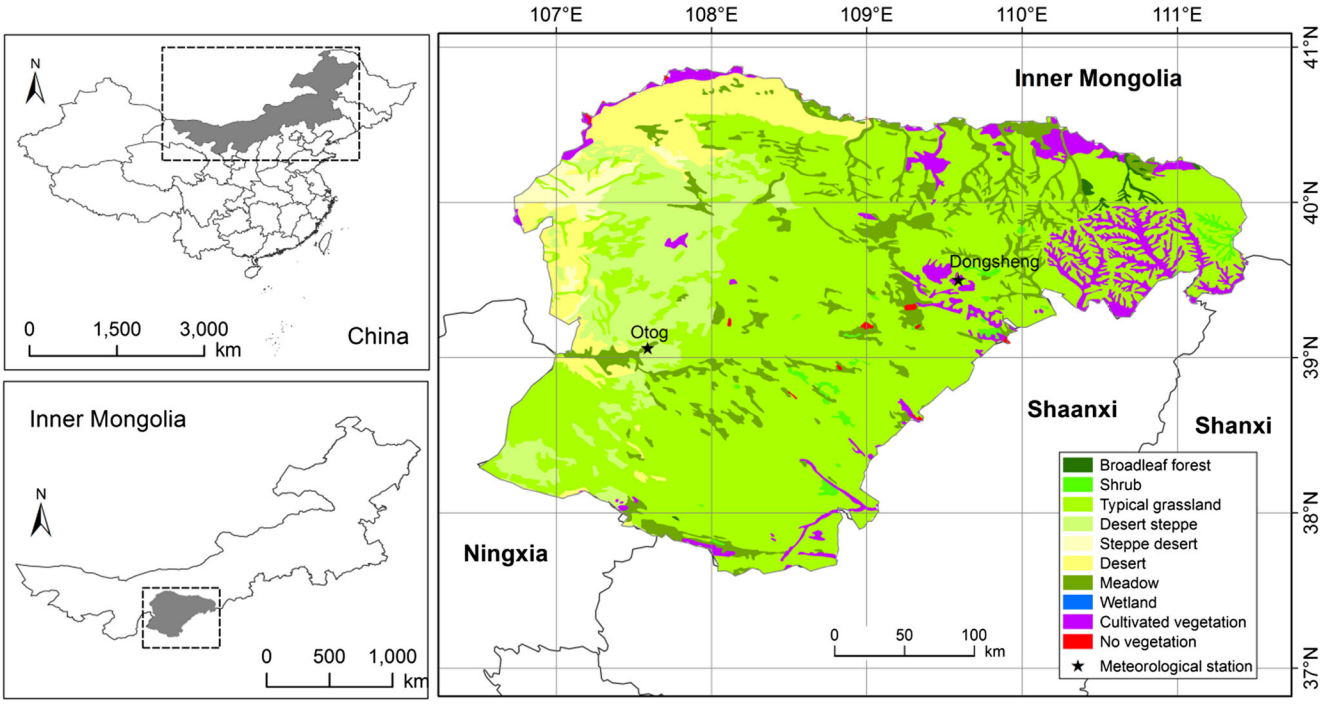

Fig. 1 Geographic location of the study area. The *inset* maps show the geographic location of the study area in Inner Mongolia, China. The main map demonstrates the spatial distribution of vegetation types

the Kubuqi Desert and the Mu Us sandy lands are distributed in this region. Grasslands play an important role in local animal and husbandry, supporting the livelihoods of local population. Due to frequent drought events, overgrazing, and natural resources exploitation, grassland degradation and desertification have become two severe environmental problems in recent decades, which are characterized by an increase in bare lands and a decrease in grasslands (Zhu et al. 2013). However, the deteriorating conditions have been reversed since 2000 as conservation policies (e.g., grain-for-green policy) and management were implemented (Meng et al. 2011).

Data sets

Our study used the newly available GIMMS3g NDVI data generated in the framework of the Global Inventory Monitoring and Modeling System (GIMMS) project at the NASA Goddard Space Flight Center. The data set was processed in a way consistent with and quantitatively comparable to NDVI generated from improved sensors such as MODIS and SPOT-4 Vegetation, and was corrected for dropped scan lines, navigation errors, data dropouts, edge-of-orbit composite discontinuities, and other artifacts (Tucker et al. 2005). The empirical mode decomposition/reconstruction method was applied to minimize the effects of orbital drift by removing common trends between the time series of Solar Zenith Angle and NDVI (Fensholt et al. 2013; Zhu and Southworth 2013). Moreover, the data set used the maximum NDVI value over a 15-day period to represent each 15-day interval to minimize corruption of vegetation signals from atmospheric effects, cloud contamination, scan angle effects, and so on, at the time of measurement (Bi et al. 2013). The data set spans from July 1981 to December 2011 and has a spatial resolution of around 8 km as well as a temporal resolution of about 15 days. Despite the corrections and temporal compositing, the GIMMS3g data set still contains residual invalid measurements, well indicated by quality flags. A pixel with less than 80 % high-quality data points (quality flag=1 or 2) or mean NDVI value less than 0.1 through the whole time span was excluded from our analysis. For the data points with "bad" quality (quality flag>2), we used a gap-filling procedure to interpolate the NDVI values of these time points adopted by Jin et al. (2013).

There are two National Standard Meteorological Stations of China within our study area, and their locations are shown in Fig. 1. The daily meteorological data from 1982 to 2008 available from the National Meteorological Information Center of China were used to study the relationships between the SOS and climatic factors. The climatic elements of each station include daily average temperatures, daily maximum temperatures, daily minimum temperatures, daily average relative humidity, daily precipitation, and daily sunshine hours. We calculated the time series of potential climatic drivers of spring phenology, which include mean spring (March, April, and May) temperature (spring T), mean spring maximum temperature (spring maxT), spring precipitation (spring P), and mean spring sunshine hours (spring SH). We devoted more attention to the relationships between spring

precipitation and the SOS utilizing precipitation data from the Climate Research Unit (CRU) at the University of East Anglia. The CRU time-series (TS) data were month-by-month variation on a spatial resolution of 0.5° with grid nodes centered on the 0.25°, and they are now available at the global scale from 1901 to 2011 (data version: CRU TS 3.21). The CRU data were constructed from monthly observations at meteorological stations across the world's land areas. Station anomalies were interpolated into 0.5×0.5° grid size and combined with an existing climatology to obtain absolute monthly values (Harris et al. 2014). There are 108 grid nodes within and surrounding our study area (Online resource 1). To match the spatial resolution of the SOS (about 8 km), we interpolated monthly precipitation data into about 8×8 km grids using the inverse distance weighted interpolation method. For interpolation of each month, we separated the 108 grid nodes for two sections: 78 for interpolation and 30 for evaluating the results (Online resource 1). A comparison between raw values and interpolated values suggest highly significant correlation and close match of the 1:1 line (Online resource 1), and thus, we can use the interpolated monthly precipitation surfaces for further analysis. The vegetation map we used to define different grassland ecosystems was derived from 1:1,000,000 scale vegetation distribution map of China. It is digitalized based on the vegetation atlas of China and available in the format of ESRI shape file (The Chinese vegetation map editing committee of Chinese Academy of Sciences 2001). These data show detailed distribution of 11 groups of vegetation types, 51 vegetation types, 833 communities, and about 2,000 dominant species. We reclassified and rasterized the map into about 8×8 grids for further analysis.

Methods

Extracting the SOS

A global function which increases the flexibility and allows the fitted function to follow a complex behavior of time series can be constructed by including a set of local functions (Eklundh and Jönsson 2012). Denoting the local functions describing the time series in intervals around the left minimum, the central maximum and the right minimum by $f_L(t)$, $f_C(t)$, and $f_R(t)$, the global function $F(t)$, which correctly models the time series in the full interval $[t_L, t_R]$, is

$$F(t) = \alpha(t) f_L(t) + [1-\alpha(t)] f_C(t) \text{ if } t_L < t < t_C \quad (1)$$

$$F(t) = \beta(t) f_C(t) + [1-\beta(t)] f_R(t) \text{ if } t_C < t < t_R \quad (2)$$

where $\alpha(t)$ and $\beta(t)$ are cut-off functions that in small intervals around $(t_L+t_C)/2$ and $(t_C+t_R)/2$, respectively, smoothly drop from 1 to 0. The local functions can be expressed as:

$$f(t) = f(t; c_1, c_2, a_1, a_2, \ldots, a_n) = c_1 + c_2 g(t; a_1, a_2, \ldots, a_n) \quad (3)$$

where $g(t;a_1,a_2,\ldots,a_n)$ denotes the basis function. c_1 and c_2 determine the base level and the amplitude, and $a_1,a_2,\ldots,a_n$ determine the shape of the basis function. Here, we used the asymmetric Gaussian (AG) function and the double logistic (DL) function as the basis function. The AG function has the form:

$$g(t; a_1, a_2, \ldots, a_5) = \begin{cases} \exp\left[-\left(\frac{t-a_1}{a_2}\right)^{a_3}\right] & t > a_1 \\ \exp\left[-\left(\frac{a_1-t}{a_4}\right)^{a_5}\right] & t \le a_1 \end{cases} \quad (4)$$

where a_1 determines the position of the maximum or minimum with respect to the independent time variable t. a_2 and a_3 determine the width and flatness of the right function half, and a_4 and a_5 determine the width and flatness of the left function half. The DL function can be formulated as:

$$g(t; a_1, \ldots, a_4) = \frac{1}{1 + exp\left(\frac{a_1-t}{a_2}\right)} - \frac{1}{1 + exp\left(\frac{a_3-t}{a_4}\right)} \quad (5)$$

where a_1 determines the position of the left inflection point. a_2 represents the rate of change. Likewise, a_3 determines the position of the left inflection point, whereas a_4 denotes the rate of change. Here, the SOS is defined as the DOY that the NDVI ratio reaches 50 % in an upward direction. The NDVI ratio ($NDVI_{ratio}(t)$), which represents the state of the ecosystem, is transformed from the NDVI:

$$NDVI_{ratio}(t) = \frac{NDVI_t - NDVI_{min}}{NDVI_{max} - NDVI_{min}} \quad (6)$$

where $NDVI_t$ is the NDVI value at time t, and $NDVI_{max}$ and $NDVI_{min}$ are the maximum and minimum values of the annual NDVI curve. A 50 % point suggests that a certain pixel has attained 50 % of its maximum greenness. The justification offered for the choice of the 50 % threshold is that the increase in greenness is believed to be most rapid at this threshold. Furthermore, the vegetation signals below this level tend to be confounded with soil reflectance (White et al. 1997, 2009; de Beurs and Henebry 2010; Cong et al. 2013).

Three statistical measures were used to evaluate the performance of these functions in removing "noises": root mean

square error (RMSE), Akaike Information Criterion (AIC), and Bayesian Information Criterion (BIC). The formula of RMSE can be written as:

$$\mathrm{RMSE} = \sqrt{\frac{1}{T}\sum_{t=1}^{T}\left(\mathrm{VI}_{\mathrm{fit}}(t) - \mathrm{VI}_{\mathrm{obs}}(t)\right)^2} \quad (7)$$

where $\mathrm{VI}_{\mathrm{fit}}(t)$ represents the smoothed value and $\mathrm{VI}_{\mathrm{obs}}(t)$ is the observed value at time t. T is the number of input data points. The AIC was used to measure the model performance by penalizing the number of parameters, whose formula can be written as:

$$\mathrm{AIC} = 2k + T[\ln(\mathrm{RSS})] \quad (8)$$

where k is the number of parameters and RSS is the residue sum of squares between the raw data and fitted data. The lower the AIC value, the preferred the model is. For the AG function, k is equal to 7 (c_1,c_2,a_1,a_2,a_3,a_4,a_5), and for the DL function, k is equal to 6 (c_1,c_2,a_1,a_2,a_3,a_4). The BIC, another measure of goodness-of-fit using Bayesian framework, was calculated as:

$$\mathrm{BIC} = T\left(\ln\left[\widehat{\sigma}^2\right]\right) + k\cdot\ln(T) \quad (9)$$

where $\widehat{\sigma}^2$ is the error variance. T and k have similar meaning as that in the AIC. The BIC penalizes parameters more strongly than AIC does.

Trend estimation

A robust trend test statistic, proposed by Vogelsang, was used to estimate the per-pixel trend in the SOS and spring precipitation from 1982–2010. This method does not require a priori knowledge as to whether the time series is stationary or non-stationary (Bi et al. 2013). The statistic is based on the following regression that is obtained by computing partial sums of the original data, y_t:

$$z_t = \beta_1 t + \beta_2\left[\frac{1}{2}\left(t^2 + t\right)\right] + S_t \quad (10)$$

where z_t=$\sum_{j=1}^{t} y_j$, S_t=$\sum_{j=1}^{t}\mu_j$, and the regressors are obtained from the formulas t=$\sum_{j=1}^{t}1$ and $\frac{1}{2}(t^2+t) = \sum_{j=1}^{t} j$. The estimated β_2 is further used to calculate the t-PS_{T} test (Fomby and Vogelsang 2002). It is robust as it is effective even when high serial autocorrelation or a unit root in the errors exists (Bi et al. 2013).

Granger causality analysis

The Granger causality techniques was applied to the time series of the SOS and climate factors of two meteorological stations to determine whether variations in climate have driven a delay or advance of the SOS. Granger causality, developed in 1960s (Granger 2007), has been widely used in economics since then and becomes popular in neuroscience within the last few years (Seth 2010). It is a powerful technique for extracting the direct functional connectivity called Granger causality (G-causality). According to G-causality, X_2 causes X_1 if the inclusion of past observations of X_2 reduce the prediction error of X_1 in a linear regression model of X_1 and X_2, as compared to a model which includes only previous observations of X_1. Suppose that the temporal dynamics of one time series X_1(t) with a length of T can be described by X_1(t) and another time series X_2(t) by a bivariate autoregressive model:

$$X_1(t) = \sum_{j=1}^{p} A_{11,j}X_1(\mathrm{t}-\mathrm{j}) + \sum_{j=1}^{p} A_{12,j}X_2(t-j) + \xi_1(t) \quad (11)$$

where p is the maximum number of lagged observations incorporated into the model, A denotes the coefficients of the model, and ξ_1 is the residuals for the time series. If the variance of ξ_1 is reduced by the inclusion of the X_2 terms, then it can be said that X_2 G-causes X_1. The magnitude of this interaction can be measured by the log ratio of the prediction error variances for the restricted (R) and unrestricted (U) models:

$$F_{2\to1} = \ln\left[\frac{\mathrm{var}\left(\xi_{1\mathrm{R}(12)}\right)}{\mathrm{var}(\xi_{1\mathrm{U}})}\right] \quad (12)$$

where $\xi_{1\mathrm{R}(12)}$ is calculated from the model excluding the $A_{12,j}$ coefficients, while the $\xi_{1\mathrm{U}}$ is derived from the full model. Bivariate G-causality can be further generalized to the multivariate case called conditional G-causality in which the G-causality of X_2 on X_1 is tested in the context of multiple additional variables X_3, …, X_n. The conditional G-causality can be estimated by multivariate autoregressive (MVAR) models. Given space limitations, the detailed description of this method can be found in Seth (2010, 2011). The G-causality is sensitive to the selection of variables, the maximum number of lagged observations, and the significance test of magnitude. We extracted the time series of the SOS for 64 pixels surrounding each of these two stations from 1982–2010. These time series were summarized by grassland types for each station: typical grassland, desert steppe, and meadow. Two types, typical grassland and meadow, exist around the Dongsheng station, while all three types exists around the Otog station. The conditional G-causality was calculated to show how climatic factors, spring T, spring maxT, spring P, and spring SH, determine the SOS.

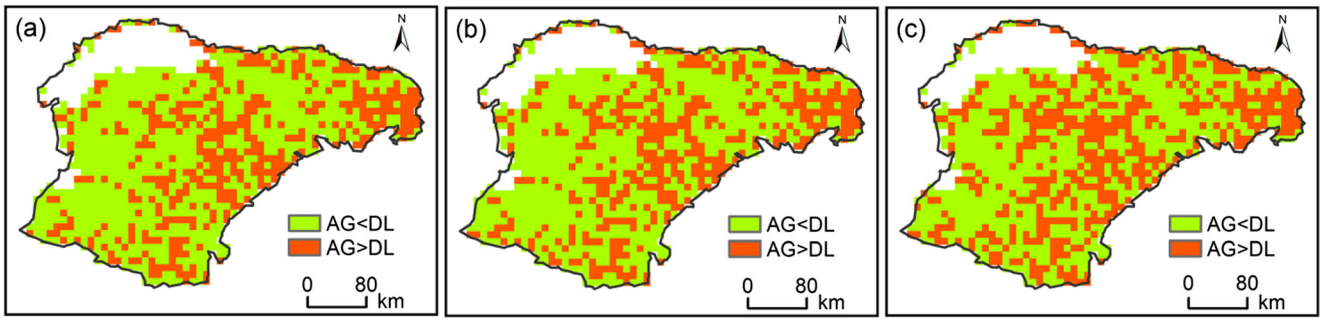

Fig. 2 Spatial pattern of the difference between the asymmetric Gaussian (*AG*) function and the double logistic (*DL*) function in terms of three statistical measures: **a** RMSE, **b** AIC, and **c** BIC

Results

Comparisons of model performance

Figure 2 shows the spatial patterns of the differences in model performance measures between the AG function and the DL function. The area where the RMSE of the AG function is larger than that of the DL function accounts for about 34.3 %, whereas the area where the RMSE of the AG function is smaller than that of the DL function makes up about 65.7 % (Fig. 2a). The area where the AIC of the AG function is larger than that of the DL function accounts for 35.2 %, while the area where the AIC of the AG function is smaller than that of the DL function occupies about 64.8 % (Fig. 2b). About 41.4 % of the study area is characterized by the larger BIC of the AG function than that of the DL function. By contrast, there is about 58.6 % of the study area where the BIC of the AG function is smaller than that of the DL function (Fig. 2c). Overall, the performance of the AG function in reducing noise of the NDVI time series is better than that of the DL function in our study area. Here, the AG function was selected to characterize the shape of complex curves of the NDVI time series.

Spatial and temporal patterns of the SOS and its change

Figure 3a demonstrates the spatial pattern of the mean SOS (1982–2010) across the study area. For the majority of the study area, the growing season starts before May. Generally, the SOS occurs earlier in the southeast than in the northwest. Figure 3b shows the spatial pattern of the coefficient of variation (CV) across the study area. The southeastern Ordos has lower CV values, implying lower variability in the SOS, whereas the northwestern Ordos has higher CV values, suggesting higher variability. Figure 3c shows the changing pattern of the SOS across the study area. No statistically significant trend is witnessed universally in the study area. Only about 3.3 % of the entire study area has an advanced trend in the SOS. Only about 2.9 % has witnessed an increased trend in the SOS, indicating a delay of the growing season start.

Relative importance of climatic drivers on the SOS

Figure 4 shows the annual variations in normalized climatic factors for the Dongsheng meteorological station. The augmented Dickey–Fuller (ADF) test, a test for a unit root in a time series, was applied to test the stationarity. The null hypothesis is that an individual time series contains a unit root against the alternative that the time series is stationary. The results show that the time series of spring T, spring maxT, spring P, and spring SH for the Dongsheng station are stationary as the null hypothesis of the ADF test is rejected (Table 1). An increasing trend in spring T, spring maxT, and spring SH is observed, whereas there is no statistically significant trend in other time series (Table 1). Figure 5 shows the annual variations in the SOS by grassland types from 1982–2008 for the Dongsheng station. The SOS indicated by the day of the year

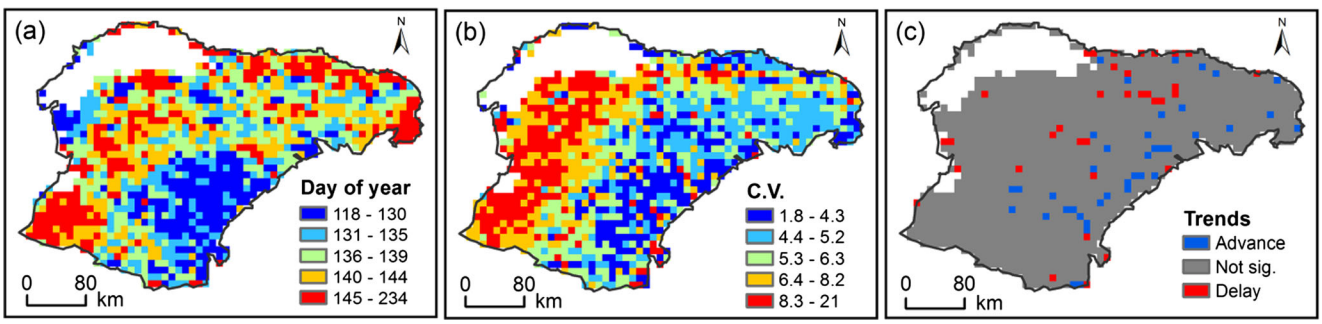

Fig. 3 Spatial pattern of **a** the mean SOS, **b** the CV for the SOS, and **c** changing trends in the SOS from 1982–2010

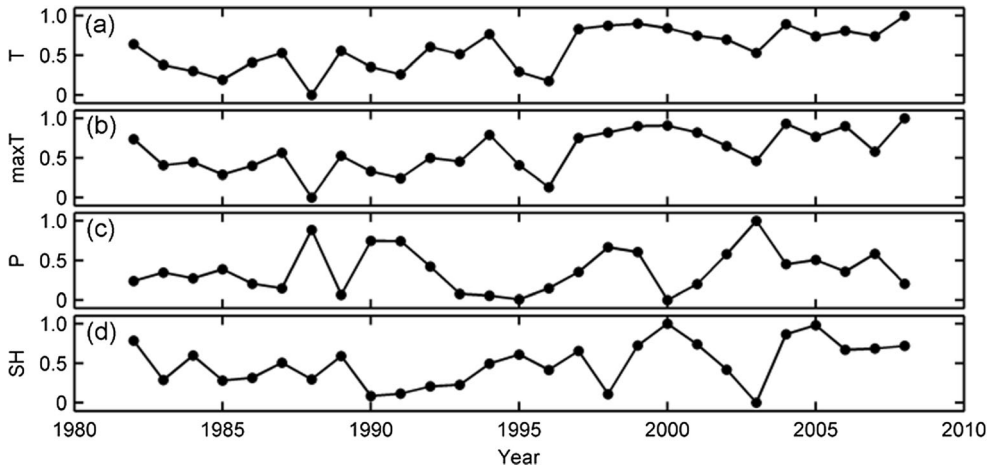

Fig. 4 Annual variations in potential drivers of the SOS at the Dongsheng station from 1982–2008: *a* spring T (mean spring temperatures); *b* spring maxT (mean spring maximum temperatures); *c* spring P (total spring precipitation), and *d* spring SH (mean spring sunshine hours). All the time series were standardized using maximum–minimum normalization

(DOY) occurs earlier over meadows (the DOY, 140) than typical grasslands (the DOY, 142). There is no significant trend in the SOS of both typical grassland and meadow surrounding the Dongsheng station. Figure 6 demonstrates the annual variations of climatic factors for the Otog meteorological station. The null hypothesis that there is a unit root is rejected for the time series of these climate factors, which implies that these time series are stationary (Table 1). An increasing trend in spring T and maxT is also observed, while no significant trend exists underlying other time series. Figure 7 shows the annual variations in the SOS by grassland types from 1982–2008 for the Otog station. The SOS occurs earlier over meadows (the DOY, 140) than typical grasslands (the DOY, 141) and desert steppes (the DOY, 143). There is no significant trend in the SOS of the three grassland types (Table 1). Table 2 reports the G-causality connectivity between climate factors and the SOS for the two stations. Higher values indicate greater causal influence of climatic factors on the SOS. As for typical grasslands surrounding the Dongsheng station, spring P has a significant influence on the SOS, as indicated by its largest magnitude value (Table 2). Other factors, spring T, spring maxT, and spring SH, have weaker influence on the SOS. The similar results were found over meadows surrounding this station. As for typical grasslands surrounding the Otog station, spring P exerts the most significant influence on the SOS, but no significant influence is found for other factors (Table 2). For meadow and desert steppe, no significant causal connectivity of climate factors with the SOS is detected, although the magnitude value for spring P is still the largest.

Table 1 Stationarity test and trend analysis for the time series of climatic factors and the SOS at the two meteorological stations (Dongsheng and Otog)

	Dongsheng		Otog	
	Stationarity	Trend	Stationarity	Trend
Spring T	Stationary	0.11[a]	Stationary	0.09[a]
Spring maxT	Stationary	0.12[a]	Stationary	0.09[a]
Spring P	Stationary	0.79	Stationary	−0.57
Spring SH	Stationary	1.57[a]	Stationary	0.14
SOS (grassland)	Stationary	0.11	Stationary	0.08
SOS (meadow)	Stationary	0.27	Stationary	−0.05
SOS (desert steppe)	–	–	Stationary	0.25

The ADF test was applied to test whether the time series is stationary

spring T mean spring temperature, *spring maxT* mean spring maximum temperature, *spring P* total spring precipitation, *spring SH* mean spring sunshine hours

[a] The trend is statistically significant

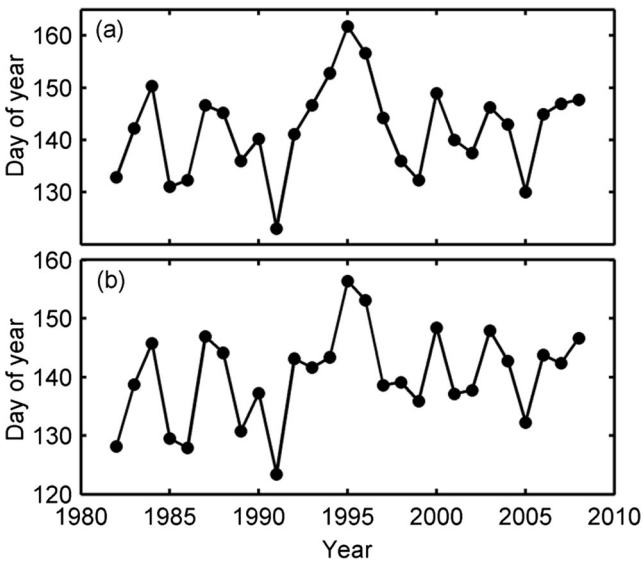

Fig. 5 Annual variations in the SOS at the Dongsheng station from 1982–2008 by grassland types: *a* typical grassland, *b* meadow

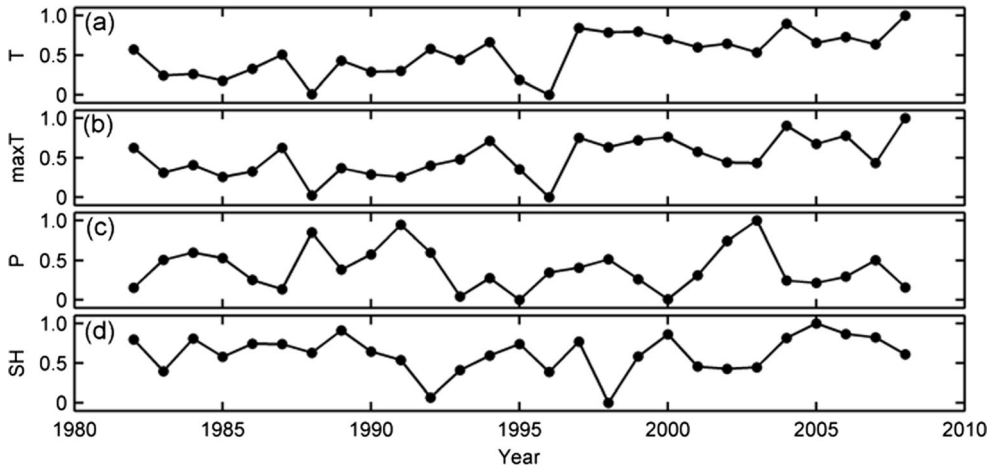

Fig. 6 Annual variations in potential drivers of the SOS at the Otog station from 1982–2008: *a* spring T (mean spring temperatures), *b* spring maxT (mean spring maximum temperatures), *c* spring P (total spring precipitation), and *d* spring SH (mean spring sunshine hours). All the time series were standardized using maximum–minimum normalization

Spatial relationships between the SOS and spring precipitation

Given that spring P is the dominant driver of the SOS in different grassland ecosystems, we devoted more attention to the relationships between the SOS and spring P spatially and temporally. Figure 8 shows the spatial pattern of correlation coefficient between the SOS and spring P across the study area. There is a universal negative correlation between the SOS and spring P, suggesting that more spring precipitation is in favor of the advance of the SOS. The correlation in the northwestern Ordos is stronger than that in the southeastern Ordos, implying that spring precipitation makes greater influence on the SOS when precipitation is less. Figure 9 shows the spatial pattern of mean spring precipitation (1982–2010). Mean spring precipitation decreases from southeast to northwest. The pattern corresponds to the spatial pattern of the SOS which is characterized by the earlier occurrence of the SOS in the southeast than in the northwest (Fig. 3a). The spatial pattern of the CV for spring precipitation is also closely related to that for the SOS, which is characterized by the lower CV for spring precipitation and the SOS in the southeast, and the higher CV the northwest (Figs. 3b and 10). Figure 11 shows the spatial pattern of the changing trend in spring precipitation from 1982–2010. Although there is a universal decreasing trend in spring precipitation with higher decreasing rate in the southeast and lower in the northwest, the trend is not statistically significant. This might be the reason why about 94.8 % of the study area shows no significant trend in the SOS from 1982–2010 given the significant importance of spring precipitation in determining the SOS (Fig. 3c).

Discussion

The accuracy and reliability of the techniques are critically important to estimate phenological metrics from remotely sensed time series whose applications are usually hindered by noise chiefly due to atmospheric conditions and sun-sensor-surface viewing geometrics (Atkinson et al. 2012). Our research evaluated the performance of two techniques in

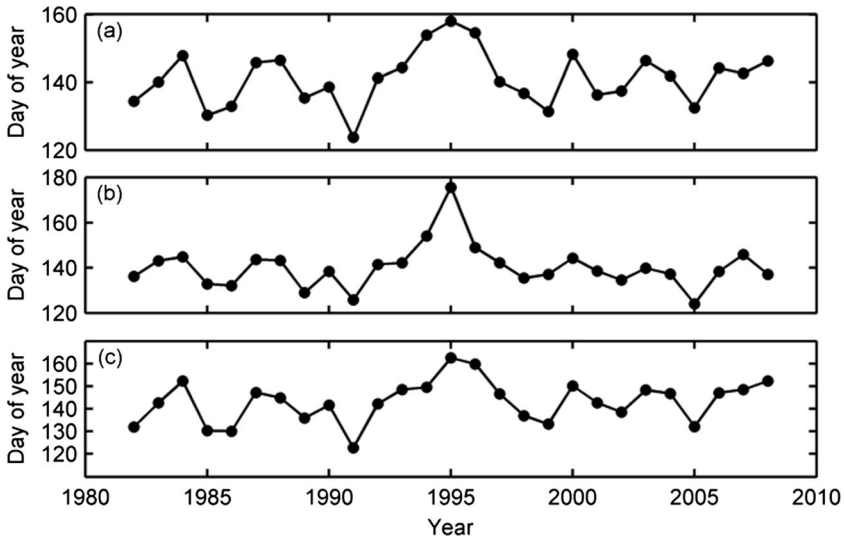

Fig. 7 Annual variations in the SOS at the Otog station from 1982–2008 by grassland types: *a* typical grassland, *b* meadow, *c* desert steppe

Table 2 G-causality connectivity between climatic factors and the SOS by grassland types for two meteorological stations (Dongsheng and Otog)

	SOS (Dongsheng)		SOS (Otog)		
	Typical grassland	Meadow	Typical grassland	Meadow	Desert steppe
spring T	0.02	0.03	0.01	0.00	0.01
spring maxT	0.02	0.02	0.01	0.00	0.02
spring P	0.18[a]	0.15[a]	0.12[a]	0.05	0.11
spring SH	0.02	0.02	0.01	0.04	0.01

spring T mean spring temperature, *spring maxT* mean spring maximum temperature, *spring P* total spring precipitation, *spring SH* mean spring sunshine hours

[a] The magnitude of connectivity is statistically significant

removing noise of the NDVI time series using three statistical measures: RMSE, AIC, and BIC. Overall, such tests pointed to the better performance of the AG function in depressing noise in grassland ecosystems of our study area. Views differ in relation to the superiority of different fitting techniques for phenology applications. Given NDVI data with identical duration, satellite correction scheme, geographic region, compositing scheme, and spatial resolution, the SOS estimates still differ with different techniques (White et al. 2009; Cong et al. 2012, 2013). Beck et al. (2006) have found that the DL function describes the NDVI data better than the AG function, as suggested by RMSE. Hird and McDermid (2009) have revealed the general superiority of the DL and AG functions by comparing to other four alternative filtering techniques: Savitzky-Golay filter, 4253H, twice filter, mean-value iteration filter, and ARMD3-ARMA5 filter. Therefore, it is critical to choose the "right" technique for specific regions depending on performance. Our research emphasizes the use of NDVI ratio, which can better represent the state of ecosystem, to detect the phenophase of spring phenology. Moreover, the increase in greenness is believed to be most rapid at 50 % threshold. This is important particularly when there is no strong a priori belief about which threshold will prove to be the "best" or most useful (Richardson et al. 2010).

Our study highlights the use of econometric models in assessing the relative importance of climatic factors on the SOS in different grassland ecosystems. We found that spring precipitation generally G-causes the SOS of different grassland types much stronger than other climatic factors in such arid and semi-arid study area. This conclusion is supported by existing studies in water-limited ecosystems which state that precipitation is considered to be an important determinant of spring phenology (Lotsch et al. 2003; Zhang et al. 2005; Piao et al. 2006). It should be noted that the G-causality of spring precipitation for meadow and desert steppe is not significant. Compared to typical grassland, meadow is a kind of azonal vegetation whose development is severely influenced by local edaphic conditions rather than climate. Meadows in our study area usually grow around the salt lakes or other water points where precipitation is not the only supply. Therefore, meadows receive relatively abundant water and are less sensitive to spring precipitation. Previous studies have also

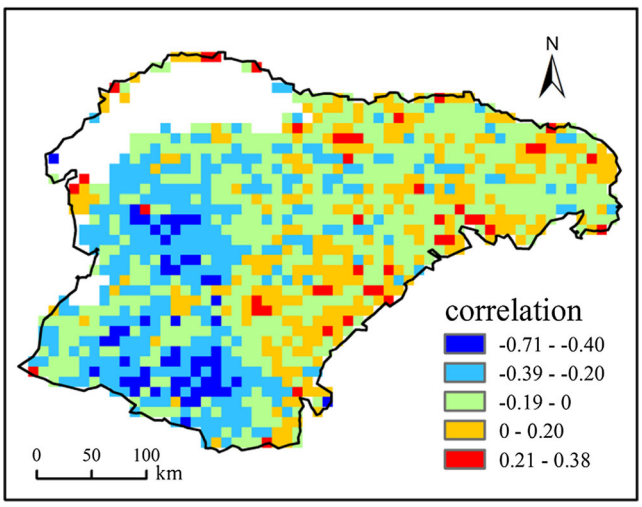

Fig. 8 Spatial pattern of the correlation coefficients between the SOS and spring precipitation

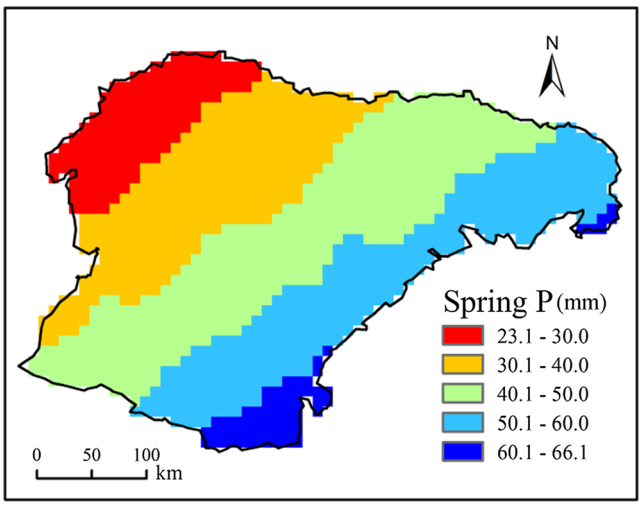

Fig. 9 Spatial pattern of mean spring precipitation (1982–2010)

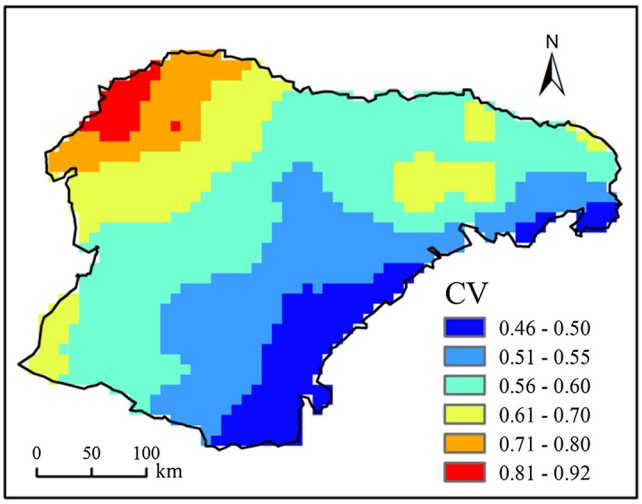

Fig. 10 Spatial pattern of the coefficients of variation for spring precipitation from 1982–2010

reported the relationships between the SOS of meadow and climate (Piao et al. 2006; Shen et al. 2011; Cong et al. 2012, 2013). Piao et al. (2006) discovered that the onset date of green-up for the alpine meadows postpones with an increase in preseason precipitation. However, Shen et al. (2011) found that increased precipitation tends to advance the SOS in alpine meadow. This might be caused by different definition of preseason cumulative precipitation. Cong et al. (2012, 2013) reported that positive but not significant correlation between the SOS and precipitation was observed. For alpine meadow, the SOS is mainly controlled by preseason temperatures, while precipitation has a little influence. Our study will further enhance and complement the understanding of spring phenology in meadows. The insignificant influence of spring precipitation on spring phenology over desert steppe does not negate the importance of water (e.g., underground water, lakes) and the impacts of other precipitation characteristics on spring

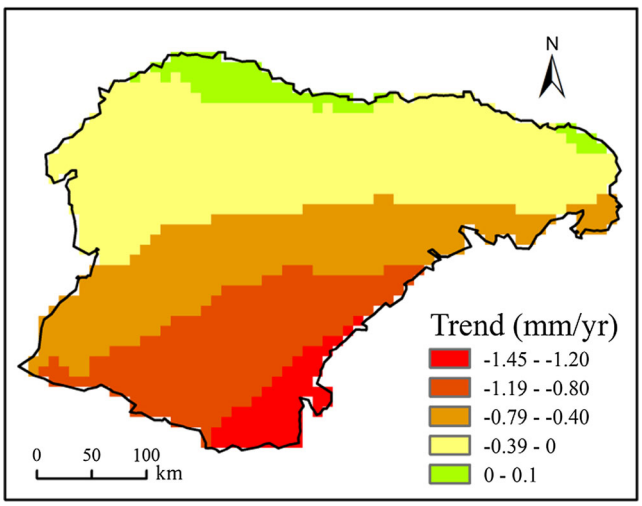

Fig. 11 Spatial pattern of the changing trends in spring precipitation from 1982–2010

phenology (e.g., timing of rainfall, rainfall frequency) (Cong et al. 2013). Desert steppe is dominated by drought-tolerant and deep-rooted grasses with small leaves and thus can reduce evapotranspiration and utilize the deep-soil water. Additionally, the first rain of spring can usually prompt germination and green-up of such grassland type. These potential drivers are not captured by total spring precipitation only. The detected weaker importance of other climatic factors does not negate their influence on the SOS through interacting with spring precipitation. Higher temperatures might induce more evaporation, faster loss of rainwater, and soil moisture deficit in water-limited ecosystems. The less water available to plants may cause the delay of the SOS (Cong et al. 2013; Wu and Liu 2013). Identifying causality in complex systems can be difficult. Correlation alone is not sufficient to establish causation, and lack of correlation does not imply lack of causation. For these reasons, the use of correlation to infer causation is risky, especially as we come to recognize that nonlinear dynamics are ubiquitous. Granger causality provides a framework which using predictability as opposed to correlation to detect causation between time-series variables.

Given the importance of spring precipitation, our research paid more attention to the linkage of the SOS and spring precipitation spatially and temporally. The spatial pattern of the gradient of the SOS from southeast to northwest is closely linked to humidity affected by the proximity to the ocean (continentality). Previous studies have also reported that the SOS is less dependent on spring precipitation in humid areas than in arid areas (Cong et al. 2012, 2013; Wu and Liu 2013). The variability of the SOS is also related to water availability, which is characterized by lower variability in more humid areas. Our research used a robust trend estimation tool with no requirement of the assumption of time-series stationarity to estimate trend. Although spring precipitation shows a widespread decreasing trend, it is not statistically significant across the study area. This corresponds to the pattern of the SOS change, characterized that only few pixels with an advance or delay of the SOS from 1982–2010 are observed in eastern Ordos. It also should be noted that changes in spring phenology result not only from the effects of climate but also from anthropogenic activities such as land-use change and land management. More studies are required to tease out the driving mechanism of these factors.

In conclusion, the spatial and temporal dynamics of the SOS (1982–2010) were derived based on the GIMMS3g NDVI data, and the conditional Granger causality measures were applied to determine the relative importance of key climatic drivers on spring phenology by grassland ecosystem types. The analysis has advantages in developing robust causal relationships through allowing important phenomena to be investigated across time. Our research found that spring precipitation plays a dominant role in determining the SOS in comparison with other climatic drivers. The spatial patterns of the SOS and its

variability are generally controlled by the corresponding patterns of spring precipitation. No statistically significant trends are observed universally, which is closely linked with the pattern of trends in spring precipitation. Our study supports existing conclusions and also reveals the characteristics of spring phenology for different grassland types in semi-arid areas. The SOS for meadow occurs earlier than that of typical grassland and desert steppe. Such a difference may be useful to landscape management (e.g., setting the grazing period) and map vegetation types. Our attention to grassland phenology will enhance and complement previous studies which make more efforts to investigate the phenology of tree species (Chen et al. 2005; Dai et al. 2013a, b; Luo et al. 2013). The research highlights the utilization of coupling remote sensing and econometric tools. It is not only valuable for understanding contemporary changes in grassland landscapes but also has great implications for predicting the effect of future climate change on vegetation phenology and further on productivity and the carbon cycling. Long-term remotely sensed time series provides promising options for characterizing the complexity of ecosystems and landscape dynamics. With the rapid increase in global change research, Granger causality method is still under development and will play a critically important role in quantifying the directional function connectivity at the intersection of remote sensing and land change science.

Acknowledgments The authors wish to thank Range Myneni, Jorge Pinzón, and Zaicun Zhu for the provision of the GIMMS3g NDVI data. We also thank Hannah Herrero for polishing English language of our manuscript. This work was supported by the National Natural Science Foundation of China under Grant No. 41371097 (PI: Dr. Jijun Meng).

References

Atkinson PM, Jeganathan C, Dash J, Atzberger C (2012) Inter-comparison of four models for smoothing satellite sensor time-series data to estimate vegetation phenology. Remote Sens Environ 123:400–417

Beck PSA, Atzberger C, Høgda KA et al (2006) Improved monitoring of vegetation dynamics at very high latitudes: a new method using MODIS NDVI. Remote Sens Environ 100:321–334

Bi J, Xu L, Samanta A et al (2013) Divergent arctic-boreal vegetation changes between north america and Eurasia over the past 30 years. Remote Sens 5:2093–2112

Chen X, Hu B, Yu R (2005) Spatial and temporal variation of phenological growing season and climate change impacts in temperate eastern China. Glob Chang Biol 11:1118–1130

Cong N, Piao S, Chen A et al (2012) Spring vegetation green-up date in China inferred from SPOT NDVI data: a multiple model analysis. Agric For Meteorol 165:104–113

Cong N, Wang T, Nan H et al (2013) Changes in satellite-derived spring vegetation green-up date and its linkage to climate in China from 1982 to 2010: a multimethod analysis. Glob Chang Biol 19:881–891

Dai J, Wang H, Ge Q (2013a) Multiple phenological responses to climate change among 42 plant species in Xi'an, China. Int J Biometeorol 57:749–758

Dai J, Wang H, Ge Q (2013b) The spatial pattern of leaf phenology and its response to climate change in China. Int J Biometeorol. doi:10.1007/s00484-013-0679-2

de Beurs KM, Henebry GM (2010) Spatial–temporal statistical methods for modelling land surface phenology. In: Hudson IL, Keatley MR (eds) Phenological research: methods for environmental and climate change analysis. Springer, Dordrecht, pp 177–208

Eklundh L, Jönsson P (2012) TIMESAT 3.1—software manual. Lund University, 82pp

Fensholt R, Rasmussen K, Kaspersen P et al (2013) Assessing land degradation/recovery in the African Sahel from long-term earth observation based primary productivity and precipitation relationships. Remote Sens 5:664–686

Fomby T, Vogelsang T (2002) The application of size robust trend statistics to global warming temperature series. J Clim 15:117–123

Ge Q, Wang H, Dai J (2013) Simulating changes in the leaf unfolding time of 20 plant species in China over the twenty-first century. Int J Biometeorol. doi:10.1007/s00484-013-0671-x

Granger CWJ (2007) Investigating causal relations by econometric models and cross-spectral methods. Econometrica 37:424–438

Harris I, Jones PD, Osborn TJ, Lister DH (2014) Updated high–resolution grids of monthly climatic observations—the CRU TS3.10 Dataset. Int J Climatol 24:623–642

Hird JN, McDermid GJ (2009) Noise reduction of NDVI time series: an empirical comparison of selected techniques. Remote Sens Environ 113:248–258

Jin C, Xiao X, Merbold L et al (2013) Phenology and gross primary production of two dominant savanna woodland ecosystems in Southern Africa. Remote Sens Environ 135:189–201

Jönsson P, Eklundh L (2002) Seasonality extraction by function fitting to time-series of satellite sensor data. IEEE Trans Geosci Remote Sens 40:1824–1832

Jönsson P, Eklundh L (2004) TIMESAT—a program for analyzing time-series of satellite sensor data. Comput Geosci 30:833–845

Lotsch A, Friedl M, Anderson B, Tucker C (2003) Coupled vegetation-precipitation variability observed from satellite and climate records. Geophys Res Lett 30:1774

Luo X, Chen X, Xu L et al (2013) Assessing Performance of NDVI and NDVI3g in monitoring leafunfolding dates of the deciduous broadleaf forest in Northern China. Remote Sens 5:845–861

Ma T, Zhou C (2012) Climate-associated changes in spring plant phenology in China. Int J Biometeorol 56:269–275

Meng J, Zhao C, Liu M (2011) Regional ecological security assessment based on land-use change: a case study of Ordos City. J Nat Resour 26:578–590

Menzel A, Fabian P (1999) Growing season extended in Europe. Nature 397:659

Menzel A, Sparks TH, Estrella N et al (2006) European phenological response to climate change matches the warming pattern. Glob Chang Biol 12:1969–1976

Myneni RB, Keeling CD, Tucker CJ et al (1997) Increasing plant growth in the northern high latitude from 1981 to 1991. Nature 386:698–702

Parmesan C, Yohe G (2003) A globally coherent fingerprint of climate change impacts across natural systems. Nature 421:37–42

Peng S, Piao S, Shen Z et al (2013) Precipitation amount, seasonality and frequency regulate carbon cycling of a semi-arid grassland ecosystem in Inner Mongolia, China: a modeling analysis. Agric For Meteorol 178–179:46–55

Piao S, Fang J, Zhou L et al (2006) Variations in satellite-derived phenology in China's temperate vegetation. Glob Chang Biol 12:672–685

Piao S, Cui M, Chen A et al (2011) Altitude and temperature dependence of change in the spring vegetation green-up date from 1982 to 2006 in the Qinghai-Xizang Plateau. Agric For Meteorol 151:1599–1608

Richardson AD, Black TA, Ciais P et al (2010) Influence of spring and autumn phenological transitions on forest ecosystem productivity. Philos Trans R Soc Lond B Biol Sci 365:3227–3246

Seth AK (2010) A MATLAB toolbox for Granger causal connectivity analysis. J Neurosci Methods 186:262–273

Seth AK (2011) Granger causal connectivity analysis: a MATLAB toolbox. University of Sussex, pp 40

Shen M, Tang Y, Chen J et al (2011) Influences of temperature and precipitation before the growing season on spring phenology in grasslands of the central and eastern Qinghai-Tibetan Plateau. Agric For Meteorol 151:1711–1722

The Chinese Vegetation Map Editing Committee of Chinese Academy of Sciences (2001) 1,000,000 scale vegetation atlas of China. Science Press, Beijing

Tucker C, Pinzon J, Brown M et al (2005) An extended AVHRR 8-km NDVI dataset compatible with MODIS and SPOT vegetation NDVI data. Int J Remote Sens 26:4485–4498

White MA, Thomton P, Running S (1997) A continental phenology model for monitoring vegetation responses to interannual climatic variability. Glob Bogeochemical Cycle 11:217–234

White MA, de Beurs KM, Didan K et al (2009) Intercomparison, interpretation, and assessment of spring phenology in North America estimated from remote sensing for 1982–2006. Glob Chang Biol 15:2335–2359

Wu X, Liu H (2013) Consistent shifts in spring vegetation green-up date across temperate biomes in China, 1982–2006. Glob Chang Biol 19: 870–880

Zhang X, Friedl MA, Schaaf CB, Strahler AH (2005) Monitoring the response of vegetation phenology to precipitation in Africa by coupling MODIS and TRMM instruments. J Geophys Res 110, D12103. doi:10.1029/2004JD005263

Zhang G, Zhang Y, Dong J, Xiao X (2013) Green-up dates in the Tibetan Plateau have continuously advanced from 1982 to 2011. Proc Natl Acad Sci U S A 110:4309–4314

Zhu L, Meng J (2010) Study on rainfall variations in the middle part of Inner Mongolia, China during the past 43 years. Environ Earth Sci 60:1661–1671

Zhu L, Southworth J (2013) Disentangling the Relationships between net primary production and precipitation in Southern Africa Savannas using satellite observations from 1982 to 2010. Remote Sens 5: 3803–3825

Zhu L, Meng J, Mao X (2013) Analyzing land-use change in farming-pastoral transitional region using autologistic model and household survey approach. Chin Geogr Sci 23:716–728